# Micelle-Dependent Spontaneous Formation of Gold(I) in Nanodendritic Chloride-Bridged Particles with Catalytic Activity for Cyclization of Alkynylanilines in Aqueous Environment

Gaganpreet Kaur,[‖†] Gaspard Hedouin,[†] Raki Mandal,[‖] Jacek B. Jasinski,[§] Xiaoqing He,[#] Min Su,[#] Juejing Liu,[‡] Xiaofeng Guo,[‡] Justin Walensky,[‖] Gary A. Baker,[‖] Fabrice Gallou,[⊥] Sachin Handa,[‖†*]

[‖]Department of Chemistry, 601 S College Ave, University of Missouri, Columbia, MO 65211, United States
[†]Department of Chemistry, 2320 S Brook St., University of Louisville, Louisville, Kentucky 40292, United States
[§]Conn Center for Renewable Energy Research, University of Louisville, Louisville, Kentucky 40292, United States
[#]Electron Microscopy Core Facility, 1030 Hitt Street, University of Missouri, Columbia, MO 65211, United States
[‡]Department of Chemistry, Washington State University, Pullman, WA 99164, United States
[⊥]Novartis Pharma AG, Basel 4056, Switzerland

*KEYWORDS. Dendrimers, nanoaggregates, micelles, gold catalysis, cyclization*

**ABSTRACT:** A proline-based engineered amphiphile featuring a thiourea functional group has been synthesized for the purpose of controlled reduction of Au(III) to Au(I) with subsequent stabilization of the resulting nanomaterial. This study elucidates the significant role played by the designer amphiphile, alongside chloride ions, in imparting a dendritic morphology to the final nanocatalyst. Such morphology is pivotal for the catalytic activity of Au(I), as demonstrated in the cyclization reaction of alkynylanilines, conducted in water as a benign reaction medium. The structural characterization of the nanomaterial revealed intriguing associations between dendritic nanocatalyst and nanomicelles, as observed through cryogenic transmission electron microscopy. Spectroscopic analyses, including X-ray photoelectron and X-ray absorption spectroscopy, corroborate the presence of Au in the +1 oxidation state within the dendritic nanomaterial. The metal-amphiphile binding is further supported by X-ray absorption fine structure analysis. Cyclic voltammetry analysis confirms the amphiphile-mediated reduction of Au(III) to Au(I). Significantly, the dendritic morphology is inaccessible when employing bromide ions, whose greater nucleophilicity disrupts the bridging linkages formed by the chloride counterpart. Under these conditions, the catalytic activity is adversely affected.

## INTRODUCTION

Unlike palladium and nickel, gold (Au) is a non-toxic metal, and it exhibits desired catalytic activity across a broad range of substrates under mild reaction conditions.[1-5] In general, ligands' expense, solvents' toxicity, and counter-anion influence remain significant considerations in catalysis.[6-12] Tailor-made ligands may be required for fine-tuning metal complexes' electronic and steric properties.[13-15] Furthermore, solvent choice profoundly impacts reaction outcomes in transition metal catalysis, including Au(I) catalysis.[7, 16] Solvents dissolve reactants, facilitating molecular interactions and influencing the stability and reactivity of intermediates in the catalytic cycle. Dipolar-aprotic solvents like dichloromethane (DCM), tetrahydrofuran (THF), dimethylformamide (DMF), and dimethyl sulfoxide (DMSO) are commonly used for their ability to dissolve diverse substrates, lower transition state energy barriers, and accommodate various functional groups.[6,17] These solvents also aid in solvating reactive intermediates and promoting crucial bond-forming steps. Hence, solvent and ligand selection are critical but often overlooked aspects of transition metal catalysis.

Ligand-free gold catalysis in water can be a promising approach in contemporary synthetic chemistry, albeit with challenges. Removing ligands compromises selectivity and efficiency, while water as a solvent introduces solubility issues, catalyst deactivation, competitive side reactions, and limited reaction scope.[14,18] In addition, catalytically inactive clumps of Au(0) are formed in the absence of an appropriate ligand. Overcoming these hurdles can enhance the environmental sustainability and operational feasibility of Au(I) catalysis. Thus, designing a benign and inexpensive amphiphile capable of serving as a ligand and solvent in gold catalysis addresses challenges associated with traditional ligands and solvents. Tailoring amphiphile structure enables the incorporation of a functional group for Au center coordination and provides a suitable solvent environment in water. The designer amphiphiles can stabilize in situ-generated nanoparticles (NPs) possessing Au(I) through a coordinating group while creating a confined reaction environment. This approach offers enhanced catalyst stability and improved selectivity through the confinement effect, promising enhanced performance and sustainability in synthetic chemistry applications.[19-22] Also, encapsulating Au NPs within micelle cores could stabilize them, preventing aggregation and preserving their properties. This stability can allow facile manipulation and, moreover, growth of NP into dendritic morphology due to a confined environment, making them versatile building blocks for advanced catalytic nanomaterials. The hydrophobic interior of micelles containing dendritic Au has the potential to promote specific interactions between reactants and catalytic sites, in

addition to increased surface area, stability against aggregation, and efficient mass transport.

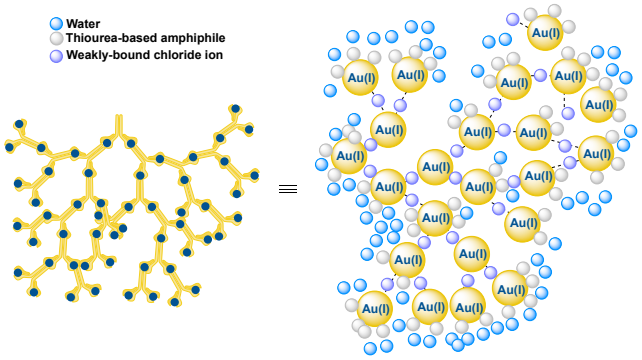


**Figure 1. Designer amphiphile assisted formation of dendritic Au(I).**

Traditionally, synthesizing dendritic Au species typically involved a controlled reduction of Au precursors in the presence of dendritic templates or stabilizers in aqueous environment.[23-24] Templates like poly(amidoamine) (PAMAM) dendrimers or polyethyleneimine (PEI) promote nucleation and growth of Au NPs with dendritic morphology.[25-28] Reduction of a Au precursor like chloroauric acid ($HAuCl_4$) with a reducing agent like sodium borohydride ($NaBH_4$) initiates NP formation on the template surface. The highly branched nature of dendritic templates promotes growth along multiple axes, forming intricate structures. However, Au NPs or dendritic Au possessing all Au in zero oxidation state are catalytically dead for reactions requiring Au(I) species.[29] However, generating dendritic Au(I) aggregates is challenging but can be achieved in the right micellar environment due to mild conditions and a highly confined environment. The inclusion of a coordinating group on the amphiphile and chloride on Au could also facilitate controlled cross-linking.[30]

To achieve catalytically active dendritic Au(I), we propose that a sulfur-containing amphiphile, driven by entropy, self-aggregates, creating a highly confined environment. Within this controlled space, a reducing amphiphile can convert Au(III) to Au(I) in a precisely regulated manner. Concurrently, these amphiphile molecules or micelles can bind with Au(I), preventing further reduction of all the Au(I) ions to Au(0). Moreover, the tightly controlled micellar microenvironment potentially promotes nucleation at the Au(I) center, fostering dendritic growth (Figure 1). Consequently, engineered micelles serve as miniature reactors, encapsulating hydrophobic Au(I) species and serving as ideal templates for synthesizing and stabilizing dendritic Au(I). The combination of micelles and dendritic Au(I) presents a synergistic nanoarchitecture with enhanced reactivity and versatility, potentially unlocking opportunities across various disciplines.

## MATERIALS AND METHODS

Our study commenced with the design and synthesis of the tailored amphiphile GG-750-M, strategically omitting thiol or sulfide functionalities while incorporating sulfur in the form of thiourea (Scheme 1A, also see Supporting Information, page S2). The resultant micellar self-assembly presents a crucial aspect, as thiol or sulfide functional groups within can inadvertently provoke uncontrolled binding and reduction of Au(III) to Au(0), posing potential interference in catalytic processes. We engineered an amphiphile integrating the thiourea functional group within its hydrophobic domain to circumvent this challenge. Notably, we selected proline as a linker bridging the hydrophilic and hydrophobic segments for several compelling reasons: firstly, its nitrogen atom serves as a pivotal component in the thiourea moiety; secondly, the cyclic structure of proline likely constrains the formation of rotamers in the Au-bound amphiphile; thirdly, it offers a site for appending the hydrophilic mPEG chain via the carboxylic acid functional group, and finally, proline's cost-effectiveness and benign nature are advantageous. Leveraging proline alongside mPEG and aliphatic amine, we successfully synthesized the designer amphiphile GG-750-M, achieving an optimal balance between its hydrophilic and lipophilic attributes, as illustrated in Scheme 1A.

The subsequent application of GG-750-M was showcased in the controlled synthesis of dendritic Au(I) species (Scheme 1B). $HAuCl_4$ was chosen as the Au(III) precursor due to its water solubility, while tetra-*n*-butyl ammonium chloride (*n*-$Bu_4NCl$) served as the phase transfer agent. Upon reaction of *n*-$Bu_4NCl$ with $HAuCl_4$, a lipophilic adduct $[AuCl_4]$-$[NBu_4]^+$ formed, releasing HCl. The possible encapsulation of this adduct within GG-750-M assemblies and the presence of thiourea functional group (a possible reductant) in the amphiphile facilitated the reduction of Au(III) to Au(I) and the oxidation of thiourea moiety, followed by the growth of dendrimers containing Au(I) (for details, see Supporting Information, pages S4-S16).

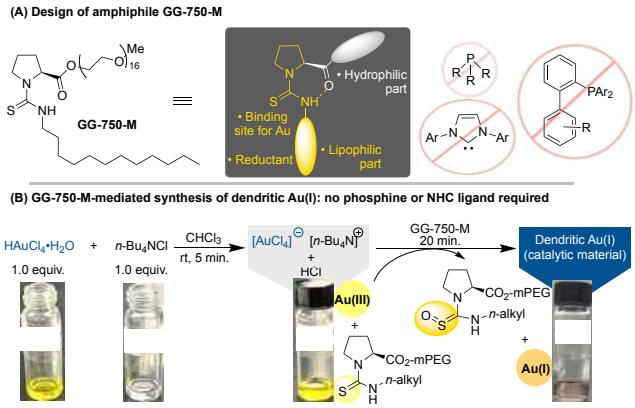


**Scheme 1. Designer amphiphile mediated growth of dendritic Au(I). (A) Design of amphiphile GG-750-M. (B) Synthesis of dendritic Au(I).**

The anticipated dendritic Au(I) species underwent comprehensive characterization using advanced analytical techniques. Cryogenic transmission electron microscopy (cryo-TEM) was employed to examine their dendritic and micellar structures. Scanning transmission electron microscopy-high angle annular dark field imaging (STEM-HAADF) was utilized for morphological analysis and particle size distribution assessment, while energy dispersive X-ray spectroscopy (EDX mapping) provided insights into the elemental

composition. Moreover, the dendritic nanomaterial underwent characterization via X-ray absorption spectroscopy (XAS) and X-ray photoelectron spectroscopy (XPS) to elucidate its coordination environment and the oxidation state of Au. While both XAS and XPS techniques offer insights into the oxidation states of each metal, XAS provides bulk analysis, while XPS offers surface-sensitive information.[31,32]

In cryo-TEM analysis, dendritic species were distinctly observed, surrounded by aqueous micelles (Figure 2 A-C, also see Supporting Information, pages S7, S8), and uniformly dispersed throughout the bulk aqueous solution. The average size of these dendritic structures fell in the 50-100 nm range, with some much larger structures observed as well. For examination of dendritic material in the solid state, STEM-HAADF analysis of the solid material was conducted (Figure 2 D-F). This analysis unveiled the presence of Au in the dendrimeric form within the nanomaterial. Further scrutiny indicated that the Au within the dendrimer was not aggregated but comprised an NP assembly of fairly uniform colloids approximately 7 nm in size (Figure 2F). The Au building blocks were slightly anisotropic, having an average length and width of 7.6 ± 1.7 nm and 5.6 ± 1.0 nm, respectively, yielding an aspect ratio of 1.4 ± 0.3 (see Supporting Information, Figure S3 on page S9). To ascertain the Au/sulfur ratio, EDX analysis was employed, revealing a 1:1 Au:S ratio, suggesting direct binding of at least one amphiphile to each surface Au(I) ion (Figure 2G). Detailed analysis also unveiled the presence of chloride ions and small atoms such as carbon, oxygen, and nitrogen within the dendritic structure (for details, see Supporting Information, page S10). XPS analysis delineated the oxidation state of Au within the dendrimer (Figure 2H), indicating an oxidation state of +1, evidenced by the binding energy at 84.2 eV.[33,34] This low binding energy was also previously reported for the $4f_{7/2}$ XPS line of Au(I).[35] However, when the material was prepared without *n*-$Bu_4NCl$, XPS analysis detected both Au(I) and Au(III) species (for details, see Supporting Information, page S11). The presence of Au(III) and Au(I) species, represented by binding energies at 86.9 eV and 84.6 eV,[33,34] respectively, may be attributed to the poor solubility of $HAuCl_4$ in the micellar interior, where the reducing functional group of the amphiphile resides. In contrast, *n*-$Bu_4NCl$ forms an adduct with $HAuCl_4$ (as depicted in Scheme 1A), facilitating its transfer into the micellar interior for subsequent reduction.

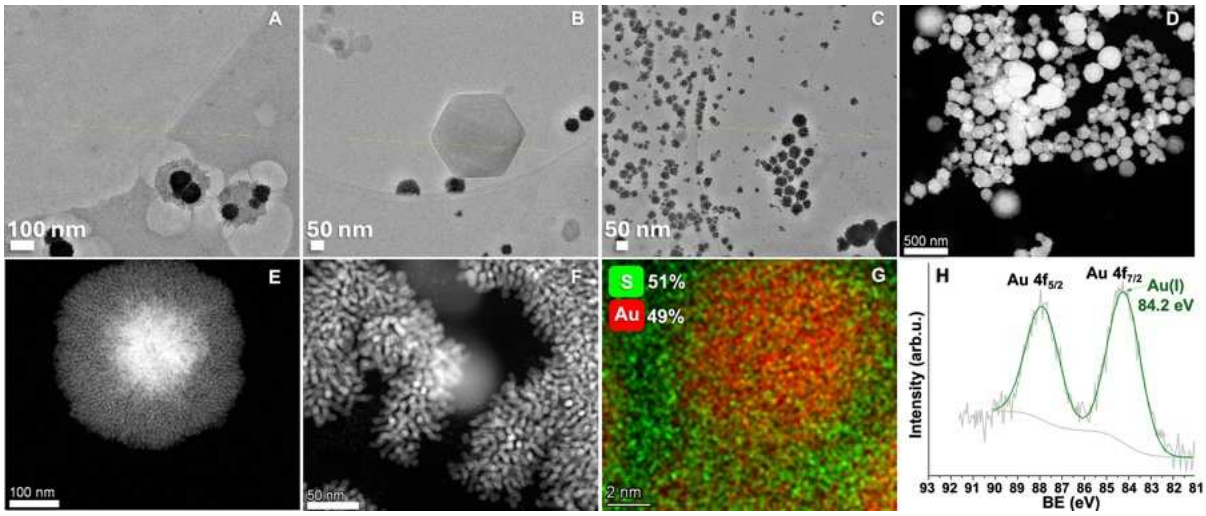


**Figure 2. Characterization of dendritic Au(I). (A-C) Cryogenic TEM images (D-F) STEM-HAADF images. (G) EDS mapping to determine Au/S ratio (H) XPS analysis.**

Au L3-edge XAS analysis was conducted to provide deeper insights into the binding dynamics between the amphiphile and Au, as well as the coordination environment of Au. The findings derived from the fitting of the Au L3-edge XAS spectra of dried nanomaterial containing dendritic Au are summarized in Figure 3 (A–E). Linear combination fitting (LCF) on the XANES region was employed on the first derivative of first derivative of the X-ray absorption near edge structure (XANES) of the Au nanomaterial, utilizing two standards: Au metal representing a valence of 0, and $Au_2S$ representing a valence of +1. This method aimed to ascertain the valence of Au and the potential phases present in the sample. The analysis revealed that the sample predominantly comprises a mixed oxidation state of 0 and +1 for Au, as depicted in Figures 3 A and B.

A zero oxidation state of Au likely correlates with the Au nanocrystals discerned through TEM analysis alongside dendritic formations. Notably, Figure 2B showcases Au(0) nanocrystals resembling hexagonal platelets. Furthermore, certain Au(0) NPs manifest as dark cores enveloped by dendritic shells, as depicted in Figures 2A, C, and E. While the LCF outcome indicates the coexistence of multiple phases within the sample, the radius distribution function (RDF), without applying phase correction (Figure 3C), unveils a complex local environment surrounding Au. Notably, four prominent RDF peaks emerge at 1.69 Å, 2.18 Å, 2.60 Å, and 2.96 Å, signifying intricate spatial arrangements. Initially, the RDF derived from the Au nanomaterial exhibits characteristics of both Au(I) and metallic (zero valent ) Au.[36] This observation is further underscored by the overlapping RDF

profiles obtained from Au NPs, Au foil, and $Au_2S$, suggesting the concurrent presence of distinct oxidation states of Au.

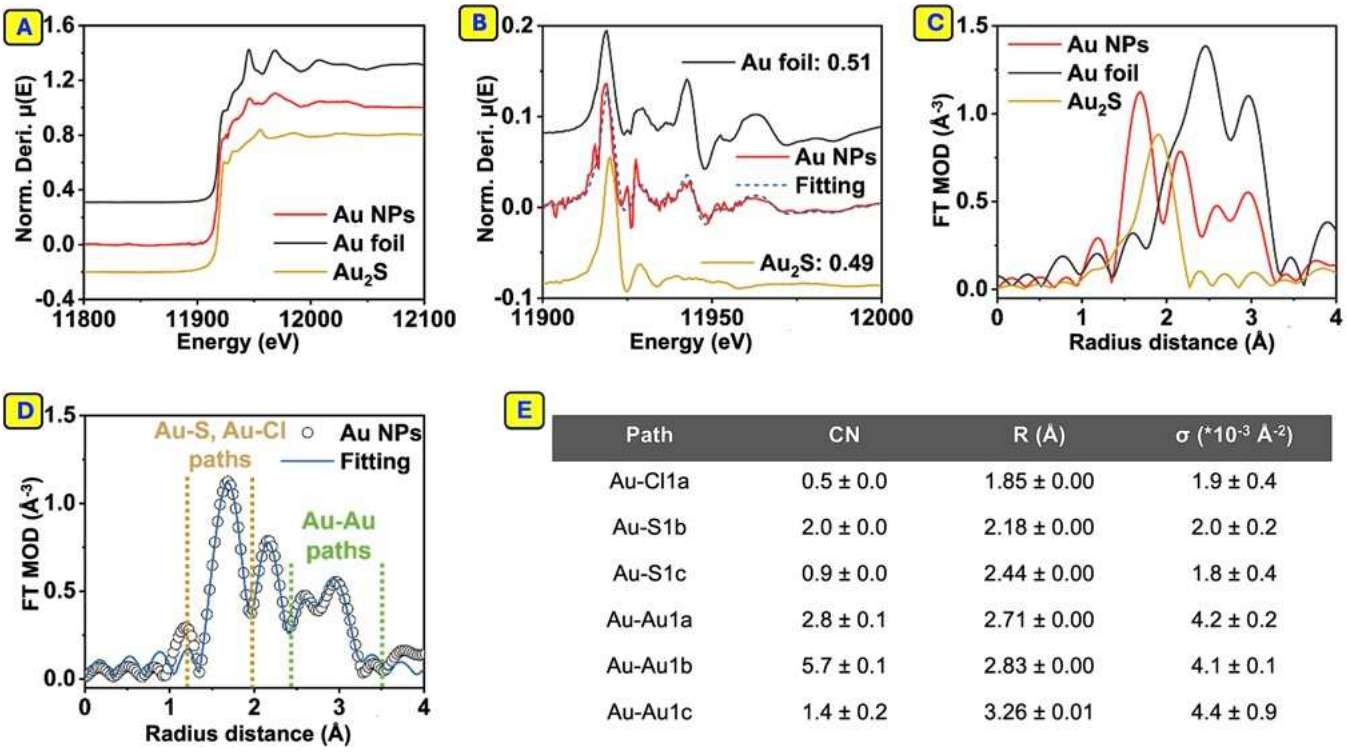


| Path | CN | R (Å) | σ (*10$^{-3}$ Å$^{-2}$) |
|---|---|---|---|
| Au-Cl1a | 0.5 ± 0.0 | 1.85 ± 0.00 | 1.9 ± 0.4 |
| Au-S1b | 2.0 ± 0.0 | 2.18 ± 0.00 | 2.0 ± 0.2 |
| Au-S1c | 0.9 ± 0.0 | 2.44 ± 0.00 | 1.8 ± 0.4 |
| Au-Au1a | 2.8 ± 0.1 | 2.71 ± 0.00 | 4.2 ± 0.2 |
| Au-Au1b | 5.7 ± 0.1 | 2.83 ± 0.00 | 4.1 ± 0.1 |
| Au-Au1c | 1.4 ± 0.2 | 3.26 ± 0.01 | 4.4 ± 0.9 |

**Figure 3. XAS analysis of nanomaterial containing dendritic Au(I): (A, B) Au XANES and linear combination fitting of edge region; (C, D) Au XAFS fitting to the FT and Au XAFS spectra; (E) best-fit parameters to the Au XAFS spectra.**

X-ray absorption fine structure (XAFS) analysis provides valuable insights into Au's local environment. Analysis of the XAFS fits suggests a multi-phase composition, prominently featuring sulfur-bound Au particles (Figure 3D, E). Specifically, the fitting results unveiled two distinct Au-S scatterings, one located at 2.18 Å with a coordination number (CN) of 2.0 and another at 2.44 Å having a CN of 0.9. Notably, the Au-S path at 2.18 Å aligns precisely with the theoretically predicted distance between Au and S in $Au_2S$, while the 2.44 Å path closely mirrors the Au-S distance observed in sulfur-bound Au in the dendritic material. Regarding Au-Au scatterings, all three sub-paths diverge from the theoretical Au-Au scatterings found in bulk Au metal at 2.95 Å. Instead, they manifest at 2.71 Å, 2.83 Å, and 3.26 Å, with corresponding CNs of 2.8, 5.7, and 1.4, respectively. Of particular note, the 2.83 Å Au-Au path precisely matches the sulfur-coated Au NPs,[37,38] while the remaining two paths likely originate from distorted Au NPs (at 2.71 Å) and Au-S molecules (at 3.26 Å), suggesting the presence of both the NP and single molecule of catalytic species in the nanomaterial. Furthermore, the observed Au-Cl distance of 1.85 Å having a CN of 0.5 indicates the linkage of Au(I) ions within the dendrimer structure via chloride ions. The relatively low coordination number also suggests the multiple bridging events facilitated by chloride ions within the dendritic material. Thus, these findings collectively indicate that the amphiphile is bound to Au(I), while chloride ions play a pivotal role in shaping the unique dendritic morphology.

Our thiourea-containing amphiphile, GG-750-M, uniquely mediated the reduction of Au(III) to Au(I), a phenomenon conclusively demonstrated through cyclic voltammetry (CV). This analysis compared the behavior of Au(III) in solutions containing GG-750-M and our previously reported non-sulfur-based amphiphile, PS-750-M.[39,40] $HAuCl_4$ was dissolved in a 0.4 M NaCl solution within a pre-dried glass vial for the CV examination. Utilizing a glassy carbon disc and Pt wire as working and counter electrodes, respectively, with an Ag/AgCl reference electrode (Figure 4A, B; for details, see Supporting Information, pages S14,S15), the electrochemical reactions were monitored. In the absence of GG-750-M, a distinct negative peak current emerged at 1.22 V, corresponding to the reduction of Au(III) to Au(0). Conversely, with the introduction of 1.0 equivalent of GG-750-M, an additional peak at 1.51 V surfaced, indicating the reduction of Au(I) to Au(0). This observation strongly supports the role of GG-750-M in mediating the formation and stabilization of Au(I). In contrast, the presence of PS-750-M micelles led to a reduction peak at 1.18 V, suggesting interaction with Au(III) but lacking evidence for Au(I) formation. Hence, the thiourea handle of GG-750-M proved to be pivotal to the formation and stabilization of Au(I). This delineation of in-situ Au(I) formation from Au(III) was exclusively observed via CV in the presence of GG-750-M, with no discernible Au(I) formation evident in the presence of PS-750-M or in the absence of amphiphiles.

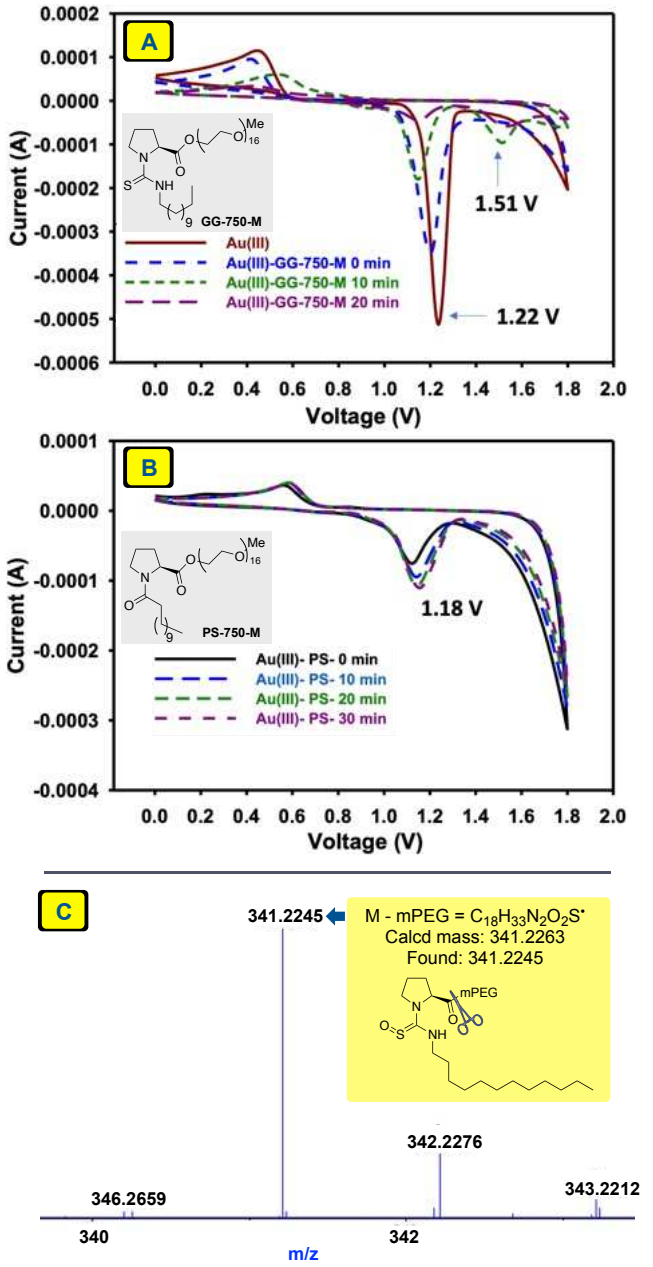


**Figure 4. Role of amphiphile in reduction of Au(III) to Au(I). (A) Cyclic voltammetry of $HAuCl_4$ in the presence of the GG-750-M amphiphile. (B) Cyclic voltammetry of HAuCl4 in the presence of PS-750-M amphiphile. (C) High-resolution mass spectrometry of dendritic Au(I): the role of GG-750-M in a controlled reduction of Au(III) to Au(I).**

The mechanism of Au(I) species formation was also investigated. It is hypothesized that this process involves a two-electron reduction mediated by the sulfur group of the thiourea moiety in the GG-750-M amphiphile. This reduction converts the thiourea group into the corresponding thiourea monoxide group, as confirmed by high-resolution mass spectrometry (HRMS) of dendritic Au(I) species containing the amphiphile. The analysis revealed a mass fragment of oxidized GG-750-M, specifically M-mPEG, at 341.2245, which substantiates the role of GG-750-M in reducing Au(III) to Au(I) (Figure 4C). Additionally, other fragments of oxidized GG-750-M containing repeated units of ethylene glycol ether were detected in the HRMS (also see Supporting Information, pages S16). Notably, the reduction of Au is controlled to +1, as the thiourea and thiourea monoxide are not strong reducing agents; a much stronger reducing agent, such as $NaBH_4$, is required for further reduction.[41]

After thoroughly characterizing the dendritic Au(I) nanomaterial, we investigated their catalytic activity in the indole-forming cyclization of alkynylaniline **1** (For details, see Supporting Information, pages S18-S21).[2,29,42,43] This transformation yields highly functionalized indoles with various functional handles, recently showcased by their applications in material science,[44-46] prompted us to examine the catalytic efficacy of our aqueous material under environmentally sustainable conditions. Typically, cationic Au species ligated with phosphine or *N*-heterocyclic carbene ligands are requisite for similar transformations,[47,48] often necessitating the use of silver salt to activate the catalyst.[49,50] However, our nanocatalyst operates efficiently without the need for a ligand and toxic organic solvent. For synthetic convenience, we employed a methodology to generate dendritic Au(I) in situ for catalytic activity. Optimal conditions were determined as 3 mol% $HAuCl_4•H_2O$, 1.0 equiv. *n*-$Bu_4NCl$, 3 wt % aq. GG-750-M, 60 °C temperature, and 1 M global concentration. After 24 h of stirring, an 85% yield of product **2** was obtained (Table 1, entry 1).

**Table 1. Optimization study for the catalytic transformation[a]**

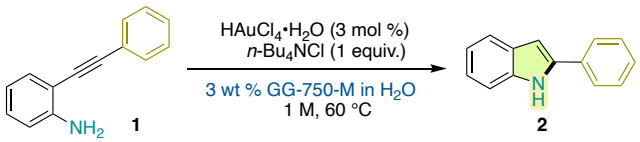


| entry | conditions | **2** (%)[b] |
|---|---|---|
| **1** | **No deviation** | **91 (85%)[c]** |
| 2 | No Au NPs | - |
| 3 | 3 mol % $HAuCl_4•H_2O$, no *n*-$Bu_4NCl$ | 30 |
| 4 | *n*-$Bu_4NBr$ instead of *n*-$Bu_4NCl$ | 12 |
| 5 | 3 mol % $AuBr_3$, instead of $AuCl_3$ | 6 |
| 6 | 3 wt % PS-750-M as solvent | 53 |
| 7 | 3 wt % Pluronic as solvent | 19 |
| 8 | 1.5 M instead of 1 M | 81 |
| 9 | 0.6 equiv. *n*-$Bu_4NCl$ instead of 1.0 equiv. | 36 |
| 10 | *n*-$(hexyl)_4NCl$ instead of *n*-$Bu_4NCl$ | 30 |
| 11 | *n*-$Et_4NCl$ instead of *n*-$Bu_4NCl$ | 50 |
| 12 | 1.0 equiv. NaBr (1 equiv.) | 50 |

[a]**Conditions. 1** (0.25 mmol), $HAuCl_4•H_2O$ (3 mol %), *n*-$Bu_4NCl$ (1 equiv.), 0.25 mL 3 wt % aq. GG-750-M, 60 °C, 24 h. [b]GCMS yield. [c]Isolated yield.

In contrast, no reaction of **1** was observed in the absence of dendritic Au (entry 2). The conversion of Au(III) to Au(I) is

sluggish without *n*-$Bu_4NCl$, which detrimentally impacted catalytic activity. In the absence of *n*-$Bu_4NCl$, the conversion rate decreased, yielding only 30% of product **2** (entry 3). Thus, chloride ions were crucial for forming dendritic Au(I) and catalytic activity. Replacing *n*-$Bu_4NCl$ with *n*-$Bu_4NBr$ resulted in only a 12% yield of product **2** (entry 4), likely due to the facile reduction of Au(III) and Au(I) to Au(0) and the reduced propensity of bromide ions to bridge with multiple Au(I) species owing to their higher nucleophilicity and larger size relative to chloride ions. Likewise, sulfide ions diminished the catalytic activity, yielding no product, and only the unreacted starting material was found in the reaction (see Supporting Information, page S18). Similarly, changing the Au source from $HAuCl_4$ to $AuBr_3$ decreased the conversion to 6% (entry 5). Other surfactants, such as PS-750-M and Pluronic, likewise were inefficient (entries 6, 7). Higher reaction concentrations diminished catalytic activity, likely due to slower exchange processes between micelles (entry 8). Reducing the amount of *n*-$Bu_4NCl$ to 0.6 equivalents decreased the yield of 2 to 36%, possibly due to the formation of fewer dendritic Au(I) structures (entry 9). Other ammonium salts proved inferior to *n*-$Bu_4NCl$, likely due to their differing lipophilicities, which may not complement the interior of GG-750-M (entries 10, 11). The addition of 1.0 equivalent of NaBr to the reaction mixture reduced the yield of 2 to 50%, likely due to dendritic structure breakdown, which is essential for catalytic activity (entry 12).

The versatility of this catalytic approach was demonstrated across a wide range of substrates, with a focus on the substitution patterns at the nitrogen atom, aniline ring, and alkyne terminus (Table 2, entries **2-23**). Both electron-donating and electron-withdrawing groups on the aniline ring exhibited excellent compatibility. Electron-releasing methyl **(4)** or electron-donating methoxy **(9)** groups yielded good-to-excellent product yields. Substrates featuring functional groups such as bromo **(5, 7, 12)**, chloro **(6, 15)**, and hydroxy **(14)** showed robust reactivity, with even the free hydroxy group in example **14** exhibiting no interference with the desired cyclization reaction. Regarding the alkyne terminus, the presence of a thiophene **(11, 12, 16)** ring was well tolerated, yielding the desired products in good-to-excellent yields Furthermore, alkyl **(14, 15, 23)**, cycloalkenyl **(13)**, aromatic **(2-10, 17-21)**, and heteroaromatic **(11, 12)** substituents were all compatible. Notably, in example **13**, the cycloalkenyl substituent remained inert, avoiding any side reactions. Beyond anilines, sulfonamide **(16-21)** and carbamate **(22)** nitrogens participated effectively in the desired reaction, affording the products in good-to-excellent yields. The nitrile functional group on the aromatic ring of the sulfonamide residue yielded 90% of the desired product **17**. Remarkably, the highly chelating dimethyl amino group of dansyl unit **21** and the pyrazole ring in **20** did not compromise the catalytic activity. Furthermore, even complex molecules, such as derivatives from the Merck Informer Library, were amenable to the reaction conditions, yielding product **23** in a 46% yield. The two thiophene rings in example **16** were also well tolerated. Thus, the broad scope of this catalytic activity, coupled with its tolerance towards various functional groups, suggested promising opportunities for further structural diversification. Notably, functional groups like chloro, bromo, hydroxy, carbamate, and ester could serve as valuable handles for such diversification efforts.

**Table 2. Substrate scope**[a]

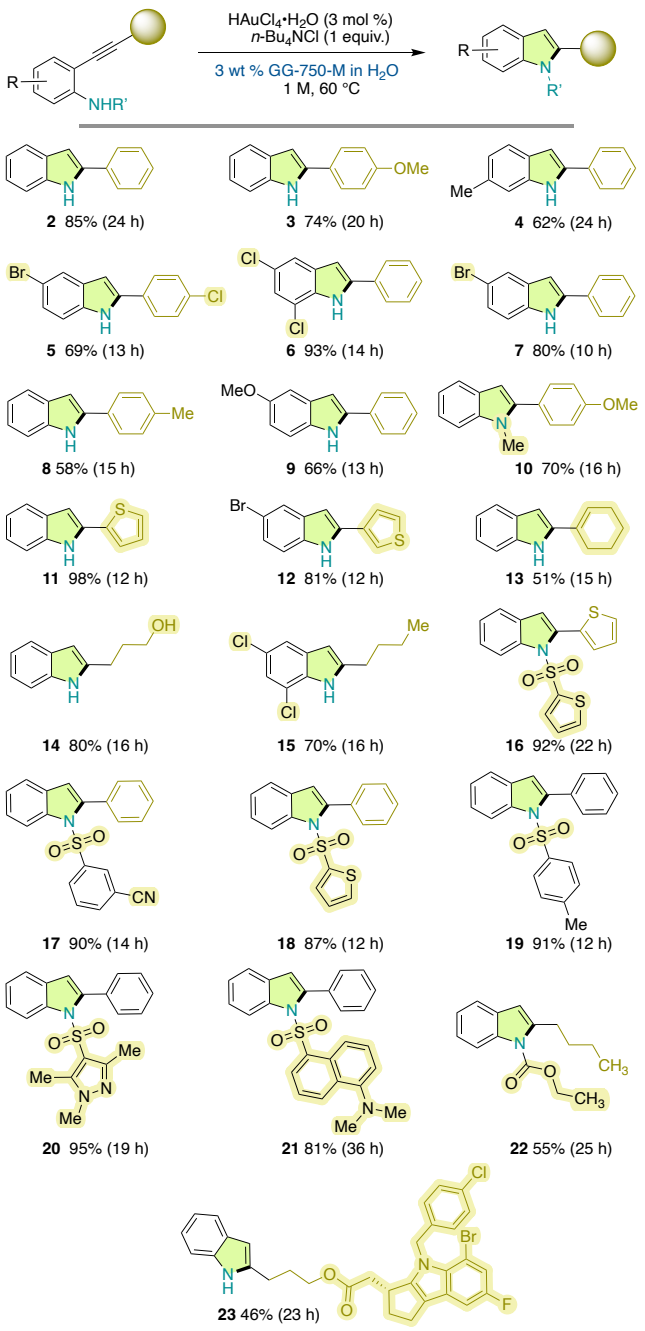


[a]**Conditions.** 2-Alkynyl anilines (0.25 mmol), $HAuCl_4•H_2O$ (3 mol %), *n*-$Bu_4NCl$ (1 equiv.), 0.25 mL 3 wt % aq. GG-750-M (0.5 mL for substrate **21** and **23**), 60 °C. All yields are isolated.

To investigate the impact of the unique dendritic morphology, the dendritic Au(I) nanomaterial was subjected to a reaction with 2.0 equivalents of NaBr (For details, see Supporting Information, page S22). It was hypothesized that the highly nucleophilic bromide ions would displace the chloride ions, thereby disrupting the bridges between Au(I)

ions and altering the dendritic structures. Subsequent analysis using HRTEM and HAADF-STEM revealed that the resulting material exhibited sparse dendritic structures alongside a predominance of small Au NPs with an average length of 3.2 ± 0.7 nm and 2.5 ± 0.5 nm width (**Figure 5**). Notably, these NPs were proven ineffective in catalyzing the cyclization reaction of **1**.

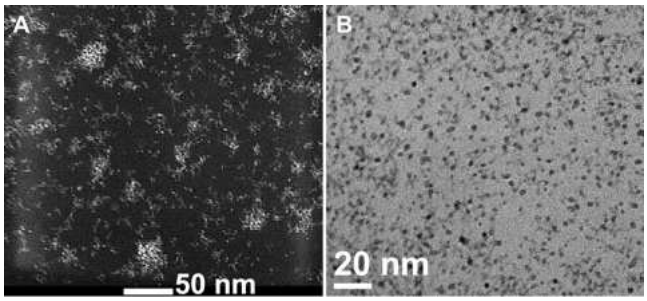


**Figure 5. Characterization of dendritic Au(I) nanomaterial after treatment with NaBr. (A) STEM-HAADF image. (B) HRTEM image.**

## CONCLUSION

The dendritic structure in the nanomaterial containing Au(I) imparts stability through chloride bridging. The resulting material exhibits high catalytic efficacy in Au(I) catalyzed reactions, particularly in aqueous environments, serving as a benign reaction medium. This capability is exemplified by its facilitation of the indole-forming valued transformation. The amphiphile GG-750-M, featuring an essential thiourea fragment, plays a pivotal role in forming the dendritic structure and maintaining the +1 oxidation state of Au. This obviates the need for harsh reductants, phosphine and carbene ligands, and toxic organic solvents in nanomaterial synthesis. The sustainability profile of the catalytic process is significantly enhanced by eschewing the use of costly ligands and organic solvents. Comprehensive spectroscopic analyses have elucidated the structure and oxidation state of Au within the nanomaterial. Additionally, cyclic voltammetry has underscored the critical role of the designer amphiphile GG-750-M in preserving the +1 oxidation state of Au. The dendritic nanomaterial is not recyclable post-catalysis. This is most likely due to the breakage of dendritic morphology after adding EtOAc or other organic solvents needed for product extraction. The catalytic material is only partially stable for an extended period, as only 55% of **2** was observed when aged nanoparticles were used.

## ASSOCIATED CONTENT

## AUTHOR INFORMATION

### Corresponding Author

*sachin.handa@missouri.edu

### Author Contributions

The manuscript was written with the contributions of all authors, and all authors have approved the final version.

### Funding Sources

S.H. is grateful to the U.S. National Science Foundation for financial support (CHE 2044778, 2345856) for the nanoparticle study.

### Supporting Information

The Supporting Information is available free of charge on the ACS Publications website. It includes details of experimental procedures, compound characterization, and analytical data.

## ACKNOWLEDGMENT

The authors acknowledge the use of Spectra 300 TEM and Krios G4 Cryo TEM at the electron microscopy core facility supported and administered by the Office of Research, Innovation, and Impact at the University of Missouri. The synchrotron measurement was performed at Hard X-ray MicroAnalysis (HXMA beamlines of the Canadian Light Source (CLS), a national research facility of the University of Saskatchewan, which was supported by the CFI, NSERC, the National Research Council (NRC), the Canadian Institutes of Health Research (CIHR), the Government of Saskatchewan, and the University of Saskatchewan. We gratefully acknowledge Jagdeep Virdi and Ramesh Choudhary for providing technical assistance in revising the manuscript.

## REFERENCES

(1) (a) Ito Y.; Sawamura, M.; Hayashi, T. Catalytic Asymmetric Aldol Reaction: Reaction of Aldehyde with Isocyanoacetate Catalyzed by a Chiral Ferrocenylphosphine–Gold (I) Complex. *J. Am. Chem. Soc.* **1986**, *108*, 6405–6406. https://doi.org/10.1021/ja00280a056. (b) Hashmi, A. S. K.; Frost, T. M.; Bats, J. W. Highly Selective Gold-Catalyzed Arene Synthesis. *J. Am. Chem. Soc.* **2000**, *122*, 11553–11554. https://doi.org/10.1021/ja005570d. (c) Hashmi, A. S. K.; Schwarz, L.; Choi, J. H.; Frost, T. M. A New Gold-Catalyzed C–C Bond Formation. *Angew. Chem., Int. Ed.* **2000**, *39*, 2285–2288. https://doi.org/10.1002/1521-3773(20000703)39:13%3C2285::aid-anie2285%3E3.0.co;2-f

(2) Hendrich, C. M.; Sekine, K.; Koshikawa, T.; Tanaka, K.; Hashmi, A. S. K. Homogeneous and Heterogeneous Gold Catalysis for Materials Science. *Chem. Rev.* **2021**, *121*, 9113–9163. https://doi.org/10.1021/acs.chemrev.0c00824

(3) Kumar, A.; Patil. N. T. Ligand-Enabled Sustainable Gold Catalysis. *ACS Sustain. Chem. Eng.* **2022**, *12*, 6900–6918. https://doi.org/10.1021/acssuschemeng.2c01213

(4) Bhoyare, V. W.; Carrizo, E. D. S.; Chintawar, C. C.; Gandon, G.; Patil, N. T. Gold-Catalyzed Heck Reaction. *J. Am. Chem. Soc.* **2023**, *145*, 8810–8816. https://doi.org/10.1021/jacs.3c02544

(5) Hashmi, A. S. K.; Hutchings, G. J. Gold Catalysis. *Angew. Chem., Int. Ed.* **2006**, *45*, 7896–7936. https://doi.org/10.1002/anie.200602454

(6) (a) Collado, A.; Nelson, D. J.; Nolan, S. P. Optimizing Catalyst and Reaction Conditions in Gold(I) Catalysis-Ligand Development. *Chem. Rev.* **2021**, *14*, 8559–8612. https://doi.org/10.1021/acs.chemrev.0c01320. (b) Matsuoka, W.; Harabuchi, Y.; Maeda, S. Virtual Ligand Strategy in

Transition Metal Catalysis Toward Highly Efficient Elucidation of Reaction Mechanisms and Computational Catalyst Design. *ACS Catal.* **2023**, *13*, 5697–5711. https://doi.org/10.1021/acscatal.3c00576

(7) Wagner, P.; Ghosh, N.; Gandon, V.; Blond, G. Solvent Effect in Gold(I)-Catalyzed Domino Reaction: Access to Furopyrans. *Org. Lett.* **2020**, *22*, 7333–7337. https://doi.org/10.1021/acs.orglett.0c02663

(8) Li, B.; Ju, Z.; Zhou, M.; Su, K.; Yuan, D. A Reusable MOF-Supported Single-Site Zinc(II) Catalyst for Efficient Intramolecular Hydroamination of *o*-Alkynylanilines. *Angew. Chem., Int. Ed.* **2019**, *58*, 7687–7691. https://doi.org/10.1002/anie.201902171

(9) Kwon, J.; Chung, J.; Byun, S.; Kim, B. M. Efficient Synthesis of Indole Derivatives via Tandem Cyclization Catalyzed by Magnetically Recoverable Palladium/Magnetite (Pd-$Fe_3O_4$) Nanocrystals. *Asian. J. Org. Chem.* **2016**, *5*, 470–478. https://doi.org/10.1002/ajoc.201500536

(10) Wong, C. M.; Vuong, K. Q.; Gatus, M. R. D.; Hua, C.; Bhadbhade, M.; Messerle, B. A. Catalyzed Tandem C-N/C-C Bond Formation for the Synthesis of Tricyclic Indoles Using Ir(III) Pyrazolyl-1,2,3-Triazolyl Complexes. *Organometallics.* **2012**, *31*, 7500–7510. https://doi.org/10.1021/om300792b

(11) SchieBl, J.; Schulmeister, J.; Doppiu, A.; Worner, E.; Rudolph, M.; Karch, R.; Hashmi, A. S. K. An Industrial Perspective on Counter Anions in Gold Catalysis: Underestimated with Respect to "Ligand Effects." *Adv. Synth. Catal.* **2018**, *360*, 2493–2502. https://doi.org/10.1002/adsc.201800233

(12) SchieBl, J.; Schulmeister, J.; Doppiu, A.; Worner, E.; Rudolph, M.; Karch, R.; Hashmi, A. S. K. An Industrial Perspective on Counter Anions in Gold Catalysis: On Alternative Counter Anions. *Adv. Synth. Catal.* **2018**, *360*, 3949–3959. https://doi.org/10.1002/adsc.201800629

(13) (a) Wang, Y.; Wang, Z.; Li, Y.; Wu, G.; Cao, Z.; Zhang, L. A General Ligand Design for Gold Catalysis Allowing Ligand-Directed Anti-Nucleophilic Attack of Alkynes. *Nat. Commun.* **2014**, *5*, 3470. https://doi.org/10.1038/ncomms4470. (b) Blanco Jaimes, M. C.; Bohling, C. R. N.; Serrano-Becerra, J. M.; Hashmi, A. S. K. Highly Active Mononuclear NAC-Gold(I) Catalysts. *Angew. Chem., Int. Ed.* **2013**, *52*, 7963–7966. https://doi.org/10.1002/anie.201210351. (c) Blanco Jaimes, M. C.; Rominger, F.; Pereira, M. M.; Carrilho, R. M. B.; Carabineiro, S. A. C.; Hashmi, A. S. K. Highly Active Phosphite Gold(I) Catalysts for Intramolecular Hydroalkoxylation, Enyne Cyclization and Furanyne Cyclization. *Chem. Commun.*, **2014**, *50*, 4937–4940. https://doi.org/10.1039/C4CC00839A

(14) Wang, W.; Hammond, G. B.; Xu, B. Ligand Effects and Ligand Design in Homogeneous Gold(I) Catalysis. *J. Am. Chem. Soc.* **2012**, *134*, 5697–5705. https://doi.org/10.1021/ja3011397

(15) Pedrazzani, R.; Pintus, A.; De Ventura, R.; Marchini, M.; Ceroni, P.; Silva López, C.; Monari, M.; Bandini, M. Boosting Gold(I) Catalysis via Weak Interactions: New Fine-Tunable Impy Ligands. *ACS Org. Inorg. Au* **2022**, *2*, 229–235. https://doi.org/10.1021/acsorginorgau.1c00052

(16) Dyson, P. J.; Jessop, P. G. Solvent Effects in Catalysis: Rational Improvements of Catalysts: Via Manipulation of Solvent Interactions. *Catal. Sci. Technol.* **2016**, *6*, 3302–3316. https://doi.org/10.1039/C5CY02197A

(17) Shahzad, S. A.; Sajid, M. A.; Khan, Z. A.; Canseco-Gonzalez, D. Gold Catalysis in Organic Transformations: A Review. *Synthetic Commun.* **2017**, *47*, 735–755. https://doi.org/10.1080/00397911.2017.1280508

(18) Sharma, S.; Gallou, F.; Handa, S. Towards a sustainable tomorrow: advancing green practices in organic chemistry. *Green Chem.* **2024**, *26*, 6289–6317. https://doi.org/10.1039/D4GC01826E

(19) Kaur, G.; Jasinski, J. B.; Gallou, F.; Handa, S. Metal-Micelle Interaction Leading to Spontaneous Formation of Ligand-Free Palladium(0) Nanoparticles: Highly Efficient Catalysis Enabling Biaryl Ketone Formation from Carboxylic Acid Derivatives. *ACS Appl. Mater. Interfaces* **2022**, *14*, 50947–50955. https://doi.org/10.1021/acsami.2c15099

(20) Kaur, G.; Kaur, K.; Handa, S. Efficient Catalysis in Dynamic Nanomicelles of PS-750-M Suspended in Water. *Curr. Opin. Green Sustainable Chem.* **2022,** *38*, 100690 https://doi.org/10.1016/j.cogsc.2022.100690

(21) Ansari, T. N.; Jasinski, J. B.; Leahy, D. K.; Handa, S. Metal-Micelle Cooperativity: Phosphine Ligand-Free Ultrasmall Palladium(II) Nanoparticles for Oxidative Mizoroki-Heck-Type Couplings in Water at Room Temperature. *JACS Au* **2021**, *1*, 308–315. https://doi.org/10.1021/jacsau.0c00087

(22) Ogulu, D.; Bora, P. P.; Bihani, M.; Sharma, S.; Ansari, T. N.; Wilson, A. J.; Jasinski, J. B.; Gallou, F.; Han-da, S. Phosphine Ligand-Free Bimetallic Ni(0)Pd(0) Nanoparticles as a Catalyst for Facile, General, Sustainable, and Highly Selective 1,4-Reductions in Aqueous Micelles. *ACS Appl. Mater. Interfaces* **2022**, *14*, 6754–6761. https://doi.org/10.1021/acsami.1c22282

(23) Bauer, P.; Mougin, K.; Faye, D.; Buch, A.; Ponthiaux, P.; Vignal, V. Synthesis of 3D Dendritic Gold Nanostructures Assisted by a Templated Growth Process: Application to the Detection of Traces of Molecules. *Langmuir* **2020**, *36*, 11015–11027. https://doi.org/10.1021/acs.langmuir.0c01857

(24) Abbasi, E.; Aval, S. F.; Akbarzadeh, A.; Milani, M.; Nasrabadi, H. T.; Joo, S. W.; Hanifehpour, Y.; Nejati-Koshki, K.; Pashaei-Asl, R. Dendrimers: Synthesis, Applications, and Properties. *Nanoscale Res Lett.* **2014**, *9*, 247. https://doi.org/10.1186/1556-276X-9-247

(25) Li, J.; Shen, M.; Shi, X. Poly(Amidoamine) Dendrimer-Gold Nanohybrids in Cancer Gene Therapy: A Concise Overview. *ACS Appl. Bio Mater.* **2020**, *3*, 5590–5605. https://doi.org/10.1021/acsabm.0c00863

(26) Frankamp, B. L.; Boal, A. K.; Rotello, V. M. Con-trolled Interparticle Spacing through Self-Assembly of Au Nanoparticles and Poly(Amidoamine) Dendrimers. *J. Am. Chem. Soc.* **2002**, *124*, 15146–15147. https://doi.org/10.1021/ja0280426

(27) Zhou, B.; Zheng, L.; Peng, C.; Li, D.; Li, J.; Wen, S.; Shen, M.; Zhang, G.; Shi, X. Synthesis and Characterization of PEGylated Polyethylenimine-Entrapped Gold Nanoparticles

for Blood Pool and Tumor CT Imaging. *ACS Appl. Mater. Interfaces.* **2014**, *6*, 17190–17199. https://doi.org/10.1021/am505006z

(28) Camarada, M. B. PAMAM Dendrimers as Support for the Synthesis of Gold Nanoparticles: Understanding the Effect of the Terminal Groups. *J. Phy. Chem. A.* **2017**, *121*, 8124–8135. https://doi.org/10.1021/acs.jpca.7b08272

(29) Carrettin, S.; Blanco, M. C.; Corma, A.; Hashmi, A. S. K. Heterogeneous Gold-Catalysed Synthesis of Phenols. *Adv. Synth. Catal.* **2006**, *348*, 1283–1288. https://doi.org/10.1002/adsc.200606099

(30) Hashmi, A. S. K.; Blanco, M. C.; Kurpejović, E.; Frey, W.; Bats, J. W. Gold Catalysis: First Applications of Cationic Binuclear Gold(I) Complexes and the First Intermolecular Reaction of an Alkyne with a Furan. *Adv. Synth. Catal*. **2006**, *348*, 709–713. https://doi.org/10.1002/adsc.200606012

(31) Ketenoglu, D. A General Overview and Comparative Interpretation on Element-Specific X-Ray Spectroscopy Techniques: XPS, XAS, and XRS. *X-Ray Spectrom*. **2022**, *51*, 422–443. https://doi.org/10.1002/xrs.3299

(32) (a) Zimmermann, P.; Peredkov, S.; Abdala, P. M.; DeBeer, S.; Tromp, M.; Müller, C.; van Bokhoven, J. A. Mod-ern X-Ray Spectroscopy: XAS and XES in the Laboratory. *Coord. Chem. Rev.* **2020**, *423*, 213466. https://doi.org/10.1016/j.ccr.2020.213466. (b) Wang, J.; Hsu, C. S.; Wu, T. S.; Chan, T. S.; Suen, N. T.; Lee, J. F.; Chen, H. M. In Situ X-Ray Spectroscopies beyond Conventional X-Ray Absorption Spectroscopy on Deciphering Dynamic Configuration of Electrocatalysts. *Nat. Commun.* **2023**, *14*, 6576. https://doi.org/10.1038/s41467-023-42370-8

(33) Li, L.; Li, Z.; Zhang, H.; Zhang, S.; Majeed, I.; Tan, B. Effect of Polymer Ligand Structures on Fluorescence of Gold Clusters Prepared by Photoreduction. *Nanoscale* **2013**, *5*, 1986–1992. https://doi.org/10.1039/c2nr33693f

(34) Vitale, F.; Fratoddi, I.; Battocchio, C.; Piscopiello, E.; Tapfer, L.; Russo, M. V.; Polzonetti, G.; Giannini, C. Mono- and Bi-Functional Arenethiols as Surfactants for Gold Nanoparticles: Synthesis and Characterization. *Nanoscale Res. Lett.* **2011**, *6,* 103. https://doi.org/10.1186/1556-276X-6-103

35) Kitagawa, H.; Kojima, N.; Nakajima, T. Studies of Mixed-Valence States in Three-Dimensional Halogen-Bridged Gold Compounds, $Cs_2AuIAuIIIX6$, (X = Cl, Br or I). Part 2. X-Ray Photoelectron Spectroscopic Study. *J. Chem. Soc. Dalton Trans.* **1991**, *11*, 3121–3125. https://doi.org/10.1039/DT9910003121

(36) Mikhlin, Y.; Likhatski, M.; Tomashevich, Y.; Romanchenko, A.; Erenburg, S.; Trubina, S. XAS and XPS Examination of the Au-S Nanostructures Produced via the Reduction of Aqueous Gold(III) by Sulfide Ions. *J. Elec. Spec. Phenomena.* **2010**, *177*, 24–29. https://doi.org/10.1016/j.elspec.2009.12.007

(37) MacDonald, M. A.; Zhang, P.; Qian, H.; Jin, R. Site-Specific and Size-Dependent Bonding of Compositionally Precise Gold-Thiolate Nanoparticles from X-Ray Spectroscopy. *J. Phys. Chem. Lett.* **2010**, *1*, 1821–1825. https://doi.org/10.1021/jz100547q

(38) López-Cartes, C.; Rojas, T. C.; Litrán, R.; Martínez-Martínez, D.; De La Fuente, J. M.; Penadés, | S; Fer-nández, A. Gold Nanoparticles with Different Cap-ping Systems: An Electronic and Structural XAS Analysis. *J. Phys. Chem. B* **2005**, *109*, 8761–8766. https://doi.org/10.1021/jp050184

(39) Hedouin, G.; Ogulu, D.; Kaur, G.; Handa, S. Aqueous Micellar Technology: An Alternative beyond Organic Solvents. *Chem. Commun.* **2023**, *59*, 2842–2853. https://doi.org/10.1039/d3cc00127j

(40) Virdi, J. K.; Dusunge, A.; Handa, S. Aqueous Micelles as Solvent, Ligand, and Reaction Promoter in Catalysis. *JACS Au.* **2024**, *4*, 301–317. https://doi.org/10.1021/jacsau.3c00605

(41) Silva, L. I. M.; Pérez-Gramatge, A.; Larrude, D. G.; Almeida, J. M. S.; Aucelio, R. Q.; da Silva, A. R. Colloids Surf. A: Physicochem. Eng. Asp. **2021**, ˆ, 126174. https://doi.org/10.1016/j.colsurfa.2021.126174

(42) Hashmi, A. S. K.; Salathe, R.; Frey, W. Gold-Catalyzed Cyclization of N-Alkynyl Carbamates. *Synlett* **2007**, *11*, 1763–1766. https://doi.org/10.1055/s-2007-982562

(43) Sun, Q.; Hubler, C.; Kahle, J.; Mackenroth, A. V.; Rudolph, M.; Kramer, P.; Oeser, T.; Hashmi, A. S. K. Cascade Reactions of Aryl-Substituted Terminal Alkynes Involving *in-situ* Generated $\alpha$-Imino Gold Carbenes. *Angew. Chem., Int. Ed.* **2024**, *63*, e202313738. https://doi.org/10.1002/anie.202313738

(44) Heckershoff, R.; Eberle, L.; May, G.; Kramer, P.; Rominger, F.; Rudolph, M.; Hashmi, A. S. K. Gold-Catalyzed Bidirectional Access to Planar Heptacyclic Benzobispyrido[1,2-*a*]Indoles and Benzobispyrrolo[1,2-*a*]Quinolines for Materials Science. *Adv. Synth. Catal.* **2022**, *364*, 3559–3566. https://doi.org/10.1002/adsc.202200708

(45) Heckershoff, R.; May, G.; Daumer, J.; Eberle, L.; Kramer, P.; Rominger, F.; Rudolph, M.; Mulks, F. F.; Hashmi, A. S. K. Entropy-Induced Selectivity Switch in Gold-Catalysis: Fast Access to Indolo[1,2-*a*]Quinolines. *Chem. Eur. J.* **2022**, *28*, e202201816. https://doi.org/10.1002/chem.202201816

(46) Hendrich, C. M.; Bongartz, L. M.; Hoffmann, M. T.; Zschieschang, U.; Borchert, J. W.; Sauter, D.; Kramer, P.; Rominger, F.; Mulks, F. F.; Rudolph, M.; Dreuw, A.; Klauk, H.; Hashmi, A. S. K. Gold-Catalysis Meets Materials Science – A New Approach to $\pi$-Extended Indolocarbazoles. *Adv. Synth. Catal.* **2021**, *363*, 549–557. https://doi.org/10.1002/adsc.202001123

(47) Tang, X. T.; Yang, F.; Zhang, T. T.; Liu, Y. F.; Liu, S. Y.; Su, T. F.; Lv, D. C.; Shen, W. B. Recent Progress in N-Heterocyclic Carbene Gold-Catalyzed Reactions of Alkynes Involving Oxidation/Amination/Cycloaddition. *Catalysts* **2020**, *10*, 350. https://doi.org/10.3390/catal10030350

(48) Dorel, R.; Echavarren, A. M. Gold(I)-Catalyzed Activation of Alkynes for the Construction of Molecular Complexity. *Chem. Rev.* **2015**, *115*, 9028–9072. https://doi.org/10.1021/cr500691k

(49) Wang, D.; Cai, R.; Sharma, S.; Jirak, J.; Thum-manapelli, S. K.; Akhmedov, N. G.; Zhang, H.; Liu, X.; Petersen, J. L.; Shi, X. "Silver Effect" in Gold(I) Catalysis: An Overlooked Important Factor. *J. Am. Chem. Soc.* **2012**, *134*, 9012–9019. https://doi.org/10.1021/ja303862z

(50) Lu, Z.; Han, J.; Hammond, G. B.; Xu, B. Revisiting the Influence of Silver in Cationic Gold Catalysis: A Practical Guide. *Org Lett.* **2015**, *17*, 4534–4537. https://doi.org/10.1021/acs.orglett.5b02224.

ToC

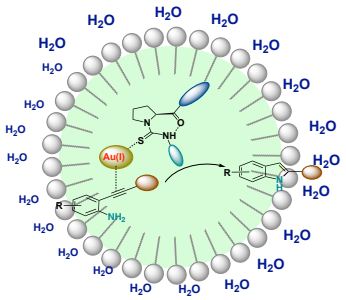


Thiourea-based designer micelle enabled the formation of dendritic Au(I) for ligand-free Au(I) catalysis in water.